Journal of Sound and Vibration 561 (2023) 117841

Contents lists available at ScienceDirect

Journal of Sound and Vibration

journal homepage: www.elsevier.com/locate/jsvi

Enhanced energy transfer and multimodal vibration mitigation in an electromechanical acoustic black hole beam

Linli Zhang [a,c], Xiang Sun [a], Jennifer Dietrich [b], Gaetan Kerschen [b], Li Cheng [a,*]

[a] Department of Mechanical Engineering, The Hong Kong Polytechnic University, Hung Hom, Kowloon, Hong Kong SAR, China
[b] Department of Aerospace and Mechanical Engineering, University of Liège, Allée de la Découverte 9, B-4000 Liège, Belgium
[c] School of Urban Railway Transportation, Shanghai University of Engineering Science, Songjiang, Shanghai, China

ARTICLE INFO

Keywords:
Acoustic black hole
Electromechanical coupling
Electrical nonlinear shunt
Energy transfer
Dynamic absorber
Multimodal vibration mitigation

ABSTRACT

Owing to their unique energy focusing capability and high-frequency damping effects, Acoustic Black Hole (ABH) structures show promise for numerous engineering applications. However, conventional ABH structures are mostly effective only above the so-called cut-on frequency, a bottlenecking deficiency that needs to be addressed if low-frequency problems are of concern. Meanwhile, achieving simultaneous high frequency ABH effects and low-frequency vibration reduction is also a challenge. In this paper, electrical linear and nonlinear shunts are intentionally added to an ABH beam via PZT patches to tactically influence its dynamics through electromechanical coupling. Both numerical and experimental results confirm that the effective frequency range of the ABH can be broadened as a result of the electrical nonlinearity induced energy transfer (ET) from low to high frequencies inside the beam. However, increased nonlinearity strength, albeit beneficial to energy transfer, jeopardizes the linear dynamic absorber (DA) effects acting on the lower-order resonances. Solutions are exploited to tackle this problem, exemplified by the use of negative capacitance in the nonlinear shunts with the embodiment of parallel linear electrical branches. On top of the nonlinear ET effects, simultaneous DA effect is also achieved for the low-frequency resonant vibration mitigation. Studies finally end up with a design methodology which embraces the principle of ET and DA to tactically cope with different frequency bands. The final outcome is the broadband multi-modal vibration reduction and the breaking down of the frequency barrier existing in conventional linear ABH structures.

1. Introduction

Acoustic Black Hole (ABH) effect has attracted sustained interests in the scientific community over the past decade due to the unique features it offers for manipulating flexural waves in thin-walled structures. Research in the area experienced a spectacular growth and triggered exciting engineering applications as reviewed in recent papers [1,2]. ABH phenomena can be materialized in a structure carrying flexural waves whose thickness profile is tailored according to a reducing power-law relationship. In the ideal scenario, the local phase and the group velocity of the propagating flexural waves gradually reduce to zero when approaching the thinnest part where the structural thickness becomes zero, so that wave reflection is annulled and the wave energy is trapped around the ABH tip [3,4]. Even in the presence of inevitable residual thickness at the tip, energy can also be effectively dissipated by using a

* Corresponding author.
E-mail address: li.cheng@polyu.edu.hk (L. Cheng).

https://doi.org/10.1016/j.jsv.2023.117841
Received 25 January 2023; Received in revised form 16 April 2023; Accepted 27 May 2023
Available online 28 May 2023
0022-460X/© 2023 Elsevier Ltd. All rights reserved.

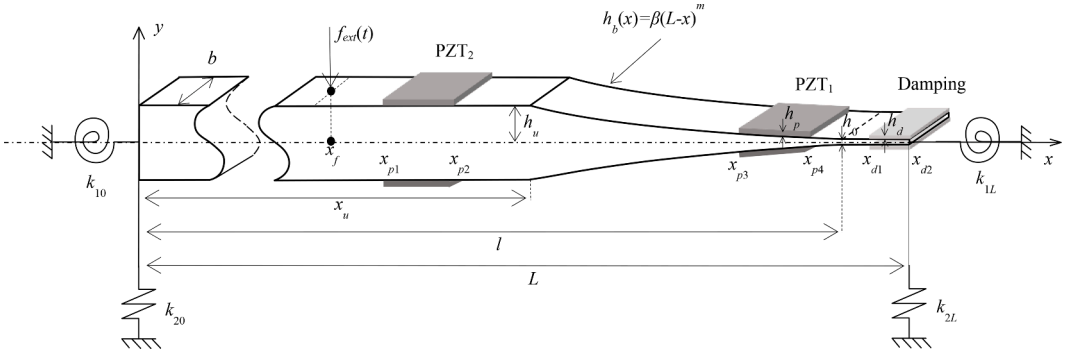

Fig. 1. An ABH beam with symmetrical and power-law thickness profile, containing a uniform platform at the tip portion. Multiple sets of piezoelectric patches, connected with external shunts, are installed as coating on both side of the beam, alongside damping layers symmetrically disposed in the tip region.

small amount of damping materials deployed as a coating over the tip area [5,6]. It is well accepted that persistent occurrence of such phenomena only takes place above the so-called cut-on frequency [7,8]. Despite this limitation, ABH offers new possibilities for conceiving lightweight and highly damped structures. The phenomena have been explored for different engineering applications such as vibration control [9,10], structural sound radiation reduction [11,12] and energy harvesting [13,14], *etc*.

Most existing research on ABH focuses on linear structures [15,16]. Even though linear ABHs exhibit remarkable and persistent energy focusing and damping enhancement at high frequencies, their deficiency at low frequencies, typically below the cut-on frequency, is still a major bottle-necking problem which hinders their applications. Reducing the frequency limit in a linear ABH structure would require an increase in the ABH size, such as the use of extended platform on the ABH tip [9] and the design of helical ABH [17] *etc.*, With limited success, these measures also affect the acceptance of the large-sized or complex structural design in engineering practice. In recent years, linear methods to enhance the low-frequency performance of ABHs were also developed, including embedding dynamic vibration absorbers in acoustic black hole plates [18] and periodic acoustic black holes [19,20], *etc.* The persistent efforts echo the increasing concerns of researchers and practitioners on the low-frequency limitation of the conventional acoustic black hole structures.

Exploration of nonlinearities (either geometric nonlinearities existing in structures or intentionally added nonlinearity) would offer a promising solution to this problem. Nonlinear systems generate harmonics [21] and can entail energy transfer from a directly excited low-frequency mode to another higher-order one [22,23]. These features have been exploited recently in ABH structures, though still largely insufficient. Typical efforts include Denis *et al.* [24] in which geometrical nonlinearities in an ABH structure were investigated. To achieve appreciable effects, the ABH wedge must be sufficiently long. Meanwhile, contact nonlinearity was also considered. Typically, a vibro-impactor was used to generate mechanical nonlinearities in an ABH beam to create effective energy transfer (ET) from low to high frequencies, thereby enhancing the passive damping effect of the ABH beam at low frequencies and achieving vibration attenuation [25,26]. However, mechanical nonlinearities through vibro-impact are difficult to control, so that the lack of tuning flexibility is also seen as a potential problem for real-life applications.

Considering the above, electrical nonlinearity was intentionally introduced in an ABH beam in our previous work [27] as a novel nonlinear energy transfer device to overcome the aforementioned limitations. It was demonstrated that a properly designed nonlinear shunt enables obvious cross-frequency energy transfer; and the transferred energy at high frequencies can be effectively dissipated through the damping of the ABH. The tuning flexibility offered by the electrical design can cater for specific structural modes in specific frequency ranges. However, it was also observed that the level of the energy transfer was limited and the direct effects on low-frequency vibration was barely observable due to the nonlinearity-impaired dynamic absorber (DA) effects. Therefore, it was difficult to conciliate the ET and DA effects simultaneously using the original shunt design [27].

Therefore, realizing enhanced cross-frequency ET while maintaining the DA effect to achieve broadband multimodal vibration mitigation is set to be the focus of this study. Enhanced ET effect would facilitate the utilization of high-frequency energy in ABH structures, either for energy harvesting or vibration control through damping dissipation. Since imposing ET is more feasible for the structural modes near the cut-on frequency of the ABH, vibration of the structure at even lower frequencies needs to be tackled via DA effect to limit the resonant vibration of lower-order modes to an acceptable level. Considering the above, this paper targets a three-fold objective: (a) providing a benchmark case to demonstrate the effects and limitations of the ET and DA effects in the existing design based on experimental evidence; (b) enhancing electromechanical coupling and ET in an ABH beam while maintaining DA effect to achieve low-frequency vibration mitigation; (c) establishing a design methodology which embraces the principle of ET and DA to tactically cope with different frequency bands.

The rest of the paper is organized as follows. An improved nonlinear electromechanical ABH model is first presented, which embodies multiple sets of damping layers and PZT patches connected to multi-branched electrical shunts with linear and nonlinear components. An ABH beam with one set of PZTs connected with the simplest nonlinear shunt is examined as a benchmark case to elucidate the effects and limitations on ET and DA, supported by experimental results. To overcome these limitations, different methods are then investigated for achieving enhanced electromechanical coupling and the subsequent energy transfer, including the

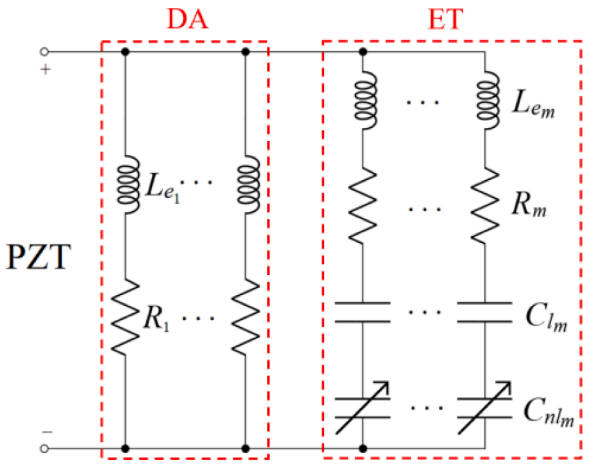

Fig. 2. Schematic diagram of multiple piezoelectric transducers with multiple-DOF nonlinear electrical shunts.

design of external circuit and the PZT layout. Additional electrical branches are added in the nonlinear shunt to maintain the DA effect without compromising the nonlinearity-induced ET effect. Finally, a design procedure, deploying different strategies for different frequency bands, is proposed. Major findings are finally summarized in the last section.

2. Theoretical model and vibration mitigation principle

Consider the beam shown in Fig. 1. The beam, with a constant width b and a total length L, is composed of a uniform portion with a constant thickness $2h_u$ and an ABH portion. The ABH portion contains a segment with a power-law profiled thickness ($2h_b$) from x_u to l, *i.e.* $h_b(x) = \beta(L\text{-}x)^m$, and an extended platform of uniform thickness h_0 till L, which enables prolonged ABH effects as demonstrated previously [9]. The beam is symmetrical with respect to the mid-line of the beam. Single or multiple piezoelectric patches and damping layers, of constant thickness h_p and h_d, respectively, are symmetrically placed on both the top and bottom surfaces of the beam. The boundary conditions of the beam are simulated by a set of rotational and translational springs on each end of the beam. In particular, assigning sufficiently large values to k_{10} (rotational stiffness) and k_{20} (translational stiffness) at the uniform end of the ABH beam, and setting the two stiffness values k_{1L} and k_{2L} to 0 at the free end would mimic a cantilever beam [28,29]. The whole system under investigation undergoes flexural vibration under a point force excitation $f_{ext}(t)$ at x_f.

External electrical modules are designed and connected to the PZT patches to form a complete set of fully coupled electromechanical system. Single- or multi-DOF linear and nonlinear electrical shunts are designed to diliver different functionalities (either for ET or DA purposes), as shown in Fig. 2.

In our previous work [27], a fully coupled electromechanical ABH model was developed via Rayleigh-Ritz approach with PZT patches connected a single-DOF nonlinear circuit. For the completeness of the study, the previous model is briefly recalled with the addition of multi-branched and multi-DOF circuits. The out-of-plane displacement $w(x, t)$ of the beam is still decomposed into a set of assumed admissible shape functions (modified trigonometric functions with supplementary boundary smoothing terms as detailed in [28]), the corresponding temporal coordinates (packed into an unknown vector $\mathbf{a}(\mathbf{t})$), the kinetic energy, potential energy and the work done by the external force $\mathbf{f}_{ext}(\mathbf{t})$ and electric charge $\mathbf{q}(\mathbf{t})$ can all be mathematically expressed to form the Lagrangian. The coupled equations can be cast into the following matrix form:

$$\begin{bmatrix} \mathbf{M} & \\ & \mathbf{L_e} \end{bmatrix} \begin{bmatrix} \ddot{\mathbf{a}}(\mathbf{t}) \\ \ddot{\mathbf{q}}(\mathbf{t}) \end{bmatrix} + \begin{bmatrix} \mathrm{Im}(\mathbf{K})/\omega & \\ & \mathbf{R} \end{bmatrix} \begin{bmatrix} \dot{\mathbf{a}}(\mathbf{t}) \\ \dot{\mathbf{q}}(\mathbf{t}) \end{bmatrix} + \begin{bmatrix} \mathrm{Re}(\mathbf{K}) + \sum_{i=1}^{m} \vec{\Theta}_i \vec{\Theta}_i^{\mathrm{T}} \big/ C_{eq_i} & -\mathbf{Z} \\ -\mathbf{Z}^{\mathbf{T}} & \mathbf{Y} \end{bmatrix} \begin{bmatrix} \mathbf{a}(\mathbf{t}) \\ \mathbf{q}(\mathbf{t}) \end{bmatrix} + \begin{bmatrix} \mathbf{0} & \\ & \mathbf{C_{nl}^{-1}} \end{bmatrix} \begin{bmatrix} \vec{\mathbf{0}} \\ \mathbf{q}^3(\mathbf{t}) \end{bmatrix} = \begin{bmatrix} \mathbf{f}_{ext}(\mathbf{t}) \\ \mathbf{0} \end{bmatrix} \tag{1}$$

where

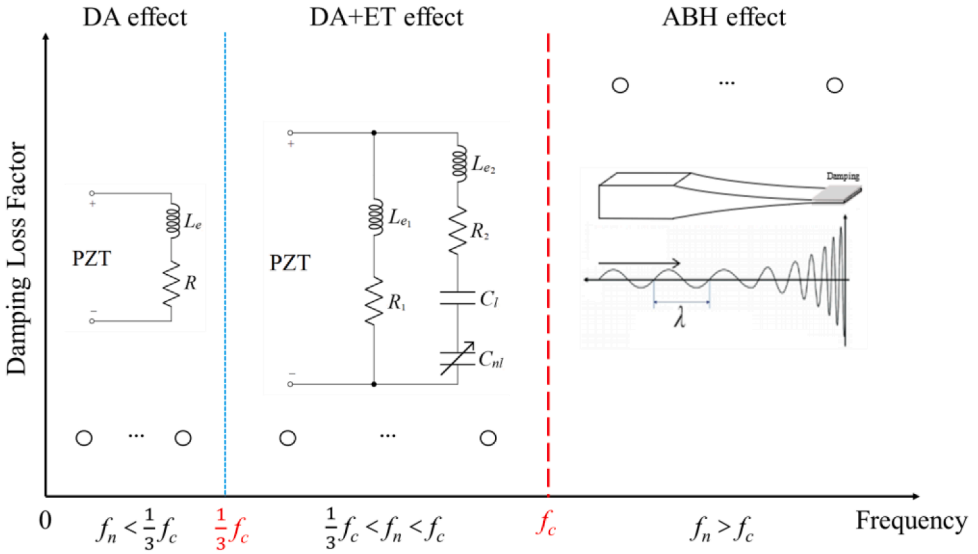

Fig. 3. Design philosophy for achieving broadband multimodal vibration mitigation and energy transfer in the electromechanical ABH beam.

$$\mathbf{L_e} = \begin{bmatrix} L_{e_1} & & & \\ & L_{e_2} & & \\ & & \ddots & \\ & & & L_{e_m} \end{bmatrix}, \mathbf{R} = \begin{bmatrix} R_1 & & & \\ & R_2 & & \\ & & \ddots & \\ & & & R_m \end{bmatrix}, \mathbf{C_{nl}} = \begin{bmatrix} C_{nl_1} & & & \\ & C_{nl_2} & & \\ & & \ddots & \\ & & & C_{nl_m} \end{bmatrix},$$

$$\mathbf{Y} = \begin{bmatrix} 1/C_{eq_1} & & & \\ & 1/C_{eq_2} & & \\ & & \ddots & \\ & & & 1/C_{eq_m} \end{bmatrix}, \vec{\mathbf{Z}} = \begin{bmatrix} \vec{\Theta}_1/C_{eq_1} & \vec{\Theta}_2/C_{eq_2} & \dots & \vec{\Theta}_m/C_{eq_m} \end{bmatrix}.$$

in which **M** and **K** with subscripts stand for different components from the mechanical ABH beam which form the global mass matrix and stiffness matrix. $\boldsymbol{\Theta}$ is the electromechanical coupling matrix and C_{eq} the capacitance of the PZT equivalent circuit. **T** denotes the transpose of a matrix. Besides, L_e is the inductance, R is the resistance and C_{nl} is the nonlinear capacitance of the external circuit.

The frequency-domain solution of this model can be obtained by Harmonic Balance Continuation method [30], coupled with a continuation strategy, proven to be effective for solving multi-DOF nonlinear systems. Meanwhile, time-domain responses can be calculated by Newmark's method, which is widely used to solve nonlinear problems, details of which are described in [31]. The above model can then be used for investigating the design of different sub-systems, in addition to optimizing the layout and location of PZT patches.

The underlying rationale which guides the electrical shunt design is schematically illustrated in Fig. 3 to cope with specific mitigation philosophies adopted for different frequency ranges. When a damping module is deployed over the ABH portion including the extended platform region, systematic ABH effects are expected above the cut-on frequency of the ABH, denoted by f_c, thus generating high damping and energy dissipation. Therefore, the high-frequency energy after f_c (inherent in this region or transferred from low frequencies to be demonstrated later) can be naturally dissipated by the ABH-enhanced damping effects. Before but not very far from f_c, ABH effect, though might still exist to some extent, is marginal and not significant enough to generate sensible vibration benefit. Therefore, external nonlinear electrical shunts are deployed in such a way that vibration energy in this frequency range can be effectively transferred to a higher frequency region (above f_c) to trigger the same energy dissipation process as the previous case. This will typically be applied to the frequency range from $1/3\ f_c$ to f_c to ensure that the dominant harmonics (starting from the third harmonic onwards) would exceed the frequency barrier imposed by f_c. In this region, the shunt design will capitalize on both ET effects, mainly achieved through nonlinear shunts and the DA effects mainly from the linear branch of the electrical circuit. For the ultra-low frequency range dominated by the resonant responses of the lower-order modes, *i.e.*, those modes with natural frequencies $f_n < 1/3\, f_c$, vibration mitigation would mainly rely on the DA effects. This is because even with ET, the transferred energy to the third harmonic would still be lower than f_c, which is still not enough to trigger meaningful ABH effects. These design principles and the achieved efficacy in terms of either EA and DA will be scrutinized hereafter.

Table 1
Material and geometrical parameters of the beam, damping, PZT and electrical shunt.

Material parameters	Geometrical parameters
Beam	Beam
Density: $\rho_b = 7800$ kg/m^3	$\beta = 0.1$
Damping loss factor: $\eta_b = 0.005$	$m = 2$
Elasticity modulus: $E_b = 210$ GPa	$b = 0.05$m
Damping	$x_u = 0.25$m
Density: $\rho_d = 950$ kg/m^3	$l = 0.45$m
Damping loss factor: $\eta_d = 0$ (specific case)	$L = 0.5$m
Elasticity modulus: $E_d = 5$GPa	$h_u = 6.25$mm
PZT	$h_0 = 0.5$mm
Density: ρ_p=7600 kg/m^3	Damping
Damping loss factor: $\eta_p = 0$	$x_{d1} = 0.48$ m (specific case)
Elasticity modulus: $E_p = 132$ GPa	$x_{d2} = 0.5$ m (specific case)
Piezoelectric stress constant: $e = -3$ C/m^3	$h_d = 0.5$ mm
Dielectric constant: $\varepsilon^s = 2.8 \times 10^{-9}$ F/m	PZT
Electrical shunt	$x_{p1} = 0.42$ m (specific case)
Inductance: L_e =1.895 H (specific case)	$x_{p2} = 0.48$ m (specific case)
Resistance: $R = 10\ \Omega$ (specific case)	$h_p = 0.5$ mm

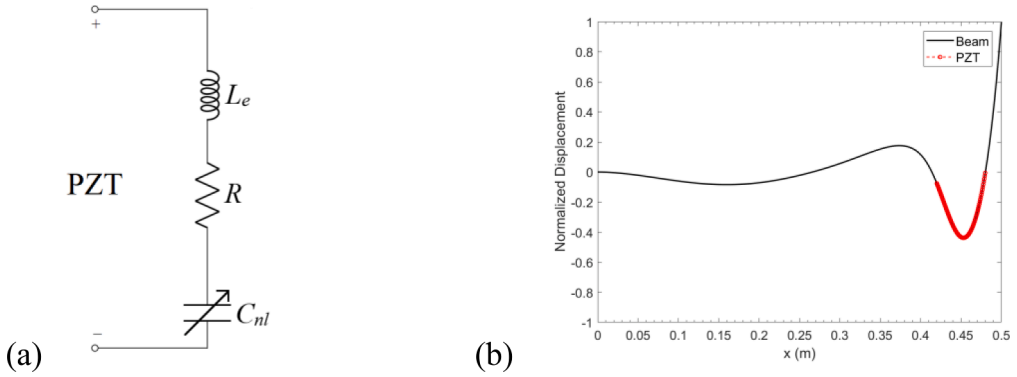

Fig. 4. (a) Schematic diagram of a nonlinear shunt to target the fourth structural mode; (b) Modal shape of the fourth mode with one set of PZTs covering the red part of the beam.

3. Numerical and experimental analyses

A cantilever ABH beam is numerically investigated. The mechanical part (ABH) has the same configuration as the one used in our previous paper [27] for easy comparisons. Material and geometrical parameters of the beam, PZT, damping and electrical shunts are listed in Table 1. The ABH beam is subjected to a harmonic point force excitation of 1 N in amplitude at the point $x_f = 0.1$ m on the uniform portion. The beam displacement, quantified by $20\log_{10}$(Displacement) expressed in dB (0 dB=1 m), is calculated at different observation positions on the beam (either on the uniform portion or the ABH portion) for structural response assessment.

3.1. Efficacy of the single branch resonant shunt

A benchmark ABH beam case, with one set of PZTs connected to the simplest nonlinear resonant shunt (Fig. 4(a)) is firstly investigated in this section to illustrate the DA effects and the corresponding nonlinear ET effects. Supplementary experiments are also conducted to verify the phenomena and showcase the existing deficiency.

In the present case, the cut-on frequency f_c of the ABH beam is 940 Hz, starting from which systematic ABH effects appear. Note f_c is slightly lower than the fifth mode (993.8 Hz) of the beam. Therefore, we choose the fourth mode before the cut-on frequency as the design and analysis target. PZT patches are placed at the position where the fourth modal deformation is the largest, *i.e.*, 0.42–0.48 m, as shown in Fig. 4(a), to generate the strongest electromechanical coupling between the PZT and the host beam. The nonlinear resonant shunt, including a linear resistance, an inductance and a cubic nonlinear capacitance, is connected to the PZTs, as shown in Fig. 4(a). Targeting the fourth mode, the corresponding inductance value is determined at around 1.9 H, which is calculated by the equivalent capacitance C_{eq} and the open-circuited angular natural frequencies ω_{oc} of the piezoelectric transducer, written as $L_e = 1/C_{eq}{\omega_{oc}}^2$ [32]. The value of the resistance and that of the nonlinear capacitance in the shunt are $R = 10\ \Omega$ and C_{nl}=1×10^{-22} C^{3}V^{-1}, respectively.

The dynamics of the ABH beam under different electrical conditions are considered: without circuit, with linear resonant circuit (C_{nl} removed) and with nonlinear circuit. Frequency response curves are obtained upon imposing a sinusoidal excitation force with an

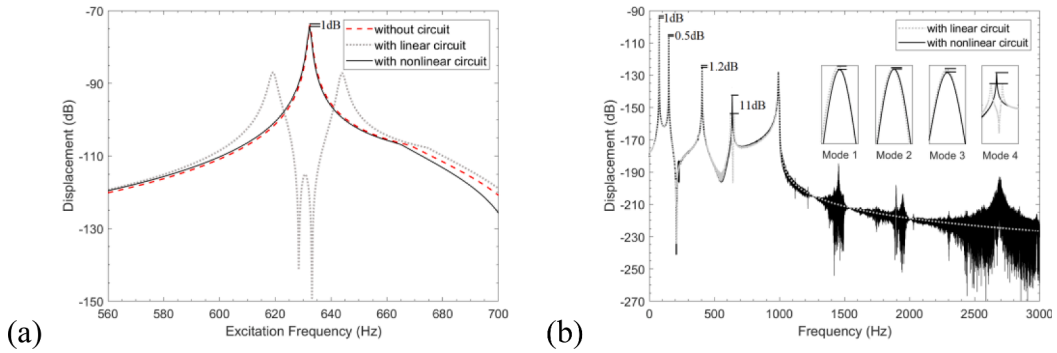

Fig. 5. Comparison of (a) beam displacements; and (b) beam displacement spectra under 0–1000 Hz sweep-frequency excitation force with different electrical circuits.

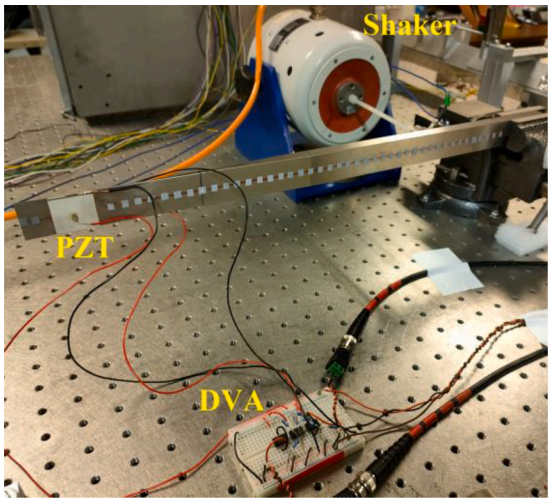

Fig. 6. Experimental setup containing the ABH beam, piezoelectric patches and digital vibration absorber.

amplitude of 1 N sweeping form 0 to 1000 Hz within 200 s. The corresponding frequency spectrum is obtained using the entire time-domain response signal through Fast Fourier Transform. Since the excitation frequency ends at 1000 Hz, vibration signals which are higher than 1000 Hz in the spectrum can be regarded as the energy transferred from the low frequencies before 1000 Hz, used as the indicator of the energy transfer phenomenon. Here, the beam displacement is measured at $x_m = 0.45$ m on the ABH portion.

Fig. 5(a) shows the close-up of the frequency-domain responses of the beam displacement around the fourth structural mode to demonstrate the influence of the linear and nonlinear circuits on the DA effect. It can be seen that, with the linear resonant shunt designed for the fourth structural mode, significant DA effect is produced on the fourth mode resonance (red dash line), with a significant amplitude reduction and peak splitting (gray dotted line). Once the strongly nonlinear capacitance is added to the linear shunt (black solid line), DA effect disappears, although the amplitude of the beam displacement is still marginally reduced (1 dB remaining) compared with the beam without external circuit. This testifies the well-known de-tuning effects of a strongly nonlinear shunt, which is not desirable as far as the DA effect is concerned. Meanwhile, the deployment of the strongly nonlinear shunt does produce obvious ET phenomena, as evidenced by the surging of the energy level beyond 1000 Hz as shown in Figure 5(b). This is obviously triggered by the nonlinearity embedded in the electrical shunt, which transfers the low-frequency energy to a higher frequency region through the creation of high-order harmonics (Detailed discussion can be found in our previous paper [27]). Coupled with high-frequency modes, ET results in an increased high frequency vibration, but for the low-frequency modes before 1000 Hz, the change in the low-order resonances is not obvious.

Experiments are conducted to verify the numerically observed phenomena. Using the benchmark case, the uniform end of the beam is clamped by a fixed bracket and the ABH end is set free as shown in Fig. 6. Due to the machining accuracy, obvious differences exist in the parameters of the beam with the numerical benchmark case. Therefore, the goal of this experiment is to verify the phenomena specific to DA and ET effect caused by the electrical shunt. We first measure the mode shape to determine the position where the fourth mode deformation is the largest, where one set of PZTs with the same length and width of 3 cm are installed on the top and bottom surfaces ($x_p = 0.43$m-0.46 m). The PZTs on both sides are first connected in series to a digital vibration absorber, and then corresponding linear and nonlinear circuits are implemented through the circuit diagram design in Simulink. Some details relating to the

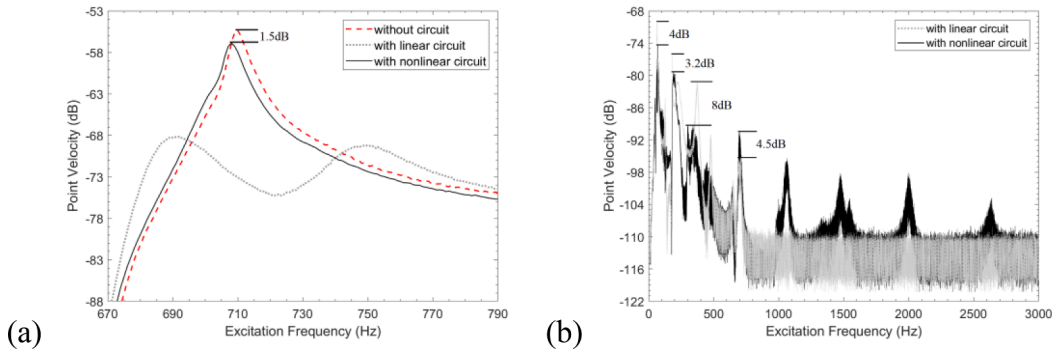

Fig. 7. Experimentally measured (a) beam velocity; and (b) beam velocity spectrum under 0–1000 Hz sweep-frequency excitation force with different electrical shunts.

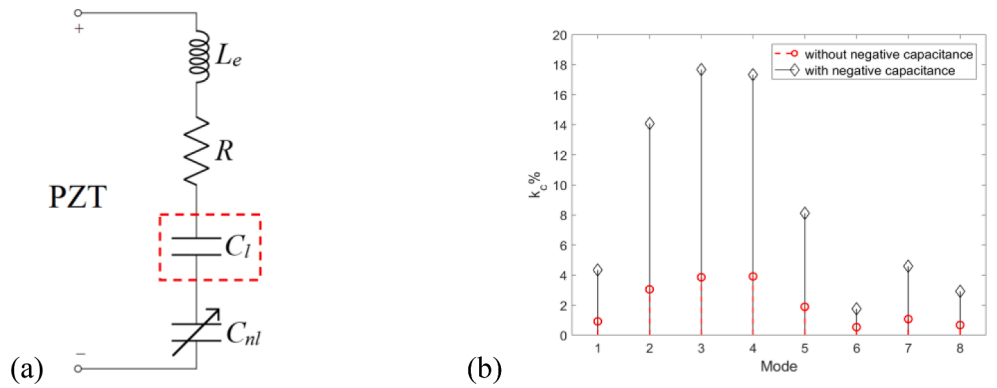

Fig. 8. (a) Schematic diagram of nonlinear shunt with a linear negative capacitance; (b) electromechanical coupling factors with and without negative capacitance.

circuit design and experiments are provided in Appendix A. More specifically, the circuit diagram and the prototype of digital vibration absorber [33] are respectively pictured in Fig. A.1 and Fig. A.2 in Appendix A. A schematic representation of the process involving an input signal (piezoelectric voltage) and an output signal (piezoelectric current) by a digital unit in Simulink is shown as Fig. A.3 in Appendix A. The beam is excited at $x_f = 0.1$ m, measured from the clamped end on the uniform portion, by an electromagnetic shaker using a sweep signal from 5 Hz to 1000 Hz. A laser vibrometer (NLV-2500) is used to measure the point velocity of the beam at $x_m = 0.35$ m on the ABH portion, which is also expressed in dB, quantified by 20log10(Point Velocity), (0 dB = 1 m/s).

An enlarged view of the beam velocity response around the fourth resonant frequency is shown in Fig. 7(a). Observed changes are consistent with numerically predicted DA effects caused by linear resonant shunt. Meanwhile, the addition of the nonlinear capacitance indeed creates the detuning phenomenon so that the DA effect is neutralized. Besides, the beam response with the nonlinear circuit is slightly reduced, which is also consistent with the numerical prediction. ET phenomenon due to electrical nonlinearity is examined using the measured beam velocity spectra, as shown in Fig. 7(b), which shows a decrease of the low-frequency vibration and, most importantly, the appearance of high-frequency energy components as an indication of the energy transfer, in agreement with previous numerical prediction. Note the flat gray area corresponding to the linear shunt case should be due to the background noise since no direct energy input is provided in that region. Therefore, the surging of the signal level over the same area after the deployment of the nonlinear shunt should be the results of the transferred energy. Therefore, experimental results basically confirm the numerically predicted phenomena relating to DA (both its birth and disappearance) and the nonlinearity-induced ET effects.

However, both numerical and experimental results suggest that, both effects remain relatively venerable and weak. The former refers to the hypersensitivity of the DA effects on the circuit design, especially the presence of the nonlinear capacitance, whilst the latter to the weak vibration reduction in the lower-order resonant peaks and much-to-improve level of the ET. All these limitations allude to the need for more sophisticated circuit design and better PZTs layout. Therefore, in the next sections, we will explore ways to enhance ET while maintaining DA effect to achieve significant broadband multimodal vibration mitigation.

3.2. *Enhancing energy transfer*

In this section, we propose to enhance the cross-frequency energy transfer through increasing the electromechanical coupling strength, by either using multiple sets of PZTs or introducing a negative capacitance in the nonlinear shunt. The electromechanical

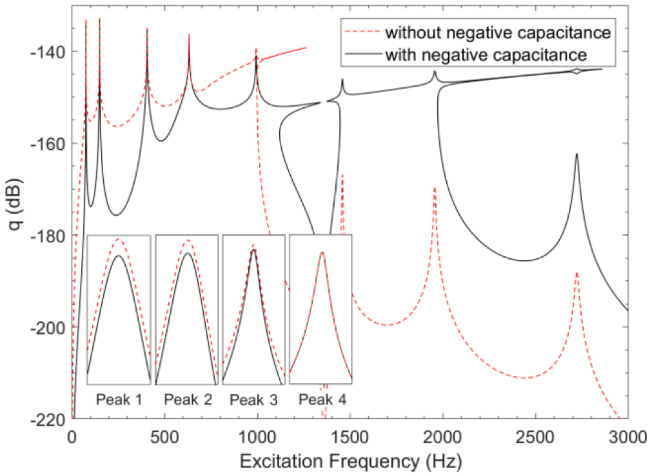

Fig. 9. Comparison of electrical charge amplitudes with and without negative capacitance.

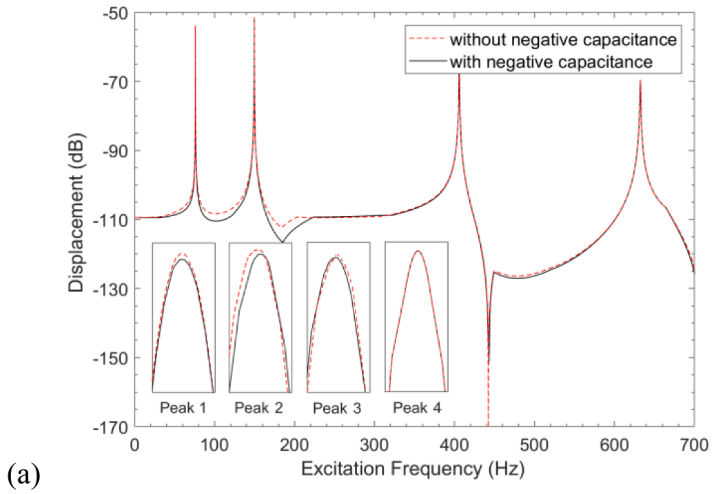

(a)

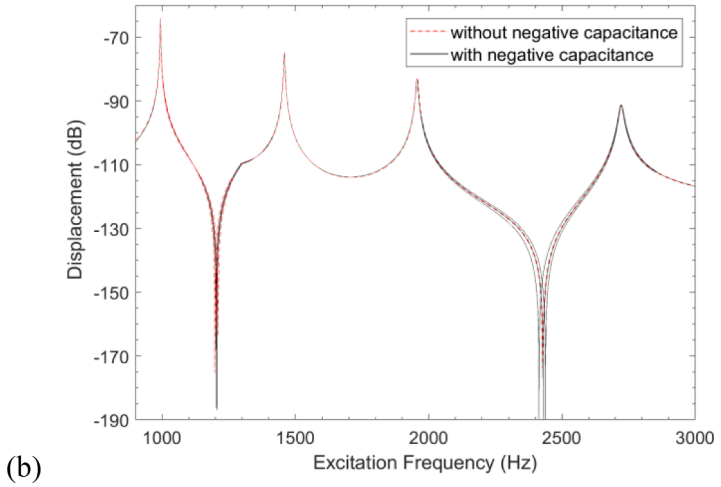

(b)

Fig. 10. Comparison of beam displacements with and without negative capacitance (a) Peak 1–4; and (b) Peak 5–8.

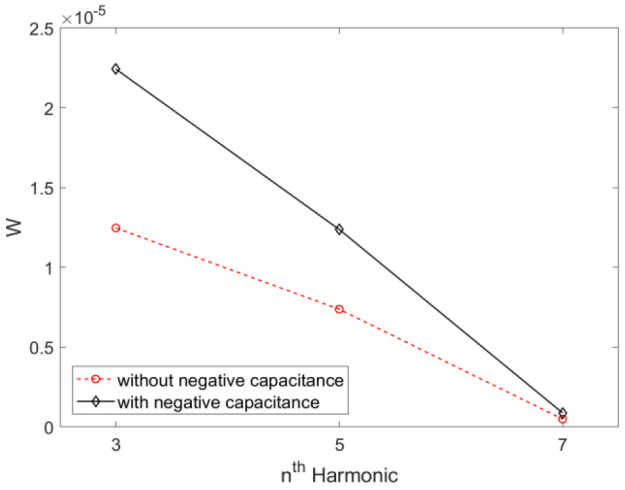

Fig. 11. Comparison of energy level in different harmonics with and without the negative capacitance.

coupling strength can be quantified using an electromechanical coupling factor k_c, $k_c^2 = (\omega_{oc}^2 - \omega_{sc}^2)/\omega_{sc}^2$ [27], which can be calculated in terms of the open-circuited and short-circuited angular natural frequencies of PZT (ω_{oc} and ω_{sc}, respectively).

It is relevant to point out that a complete ABH process involves two concurrent stages: an effective energy trapping because of slow wave effects, followed by effective energy dissipation in the ABH region to prevent the trapped energy from being bounced back. While the former is an intrinsic property of the ABH beam, the latter can be easily achieved using damping materials. To separate the two physical processes, the following analyses (unless otherwise stated) will use an ABH beam containing the so-called damping layers but with a zero-damping factor. Therefore, the co-called damping layers in this case only contribute to the added mass and stiffness to the system, but not the damping.

3.2.1. Single PZT pair with negative capacitance in the shunt

Even with a single set of piezoelectric transducers, electromechanical coupling strength can be enhanced through proper shunt design, such as adding a negative capacitance to the shunt, which is examined as the first possibility hereafter. Taking the same linear resistance and the nonlinear capacitance used in the benchmark case, the linear inductance value is changed to 0.1H with the addition of a linear negative capacitance $C_l = -3.57 \times 10^{-8}$C/V. This set of parameters results in the same resonant frequency of the electrical shunt as the benchmark case, still targeting the fourth mode of the beam. The circuit diagram is shown in Fig. 8(a) with the corresponding k_c depicted in Fig. 8(b) for each mode, which shows an obvious increase in k_c for all structural modes.

Comparisons are made in terms of the frequency responses in both mechanical and electrical systems with and without the linear negative capacitance to understand the consequences of the enhanced electromechanical coupling on the nonlinear features of the coupled system. Fig. 9 shows the effect on electrical charge q collected from the PZT patches. Several typical changes are noteworthy. More specifically, the linear negative capacitance results in a more obvious hardening phenomenon on the targeted fourth mode due to the cubic nonlinear capacitance. More specifically, the frequency of the electrical resonance peak further increases and bends to higher frequency. Meanwhile, the range of the branch formed by the bending also becomes larger, which is coupled with the high-frequency resonance peaks. This, in turn, leads to a significant increase in the high-frequency response amplitude, suggesting enhanced ET effect between adjacent modes because of the enhanced electromechanical coupling. Overall, through the enhanced electromechanical coupling effect, the electrical shunt experiences more significant hardening near its resonant frequency and leads to stronger energy transfer from low frequencies to high frequencies. Meanwhile, it can also be noticed that the amplitude reduction of the first four low-frequency resonance peaks is rather marginal as indicated by the insets of Fig. 9.

Corresponding changes in the mechanical system, in terms of displacement response of the beam, are shown in Fig. 10. Firstly, focusing on the low-frequency range (the first four resonance peaks before the cut-on frequency) shown in Fig. 10(a), we observe that the vibration amplitude reduction is rather trivial, like the amplitude charges observed in the electrical signal. As to be discussed later, this is to be ameliorated through introducing DA effects in the shunt. Besides, for the high-frequency range in Fig. 10(b), due to the enhanced electromechanical coupling, nonlinear phenomena on the beam also become stronger, like the charge signal. In particular, the bended branch observed in the electrical charge response also appears in the beam response as an isolated loop as shown in Fig. 10 (b). Therefore, with the inclusion of a linear negative capacitance in the shunt, the frequency range of the nonlinear loop increases, which also results in an increase of the beam vibration at high frequencies. This also echoes the fact that the expected enhancement in the energy transfer from the low-frequency modes to adjacent high-frequency modes is taking place.

From a different perspective, we analyze the influence of the enhanced electromechanical coupling on ET in the mechanical system by comparing the energy contained in different high-order harmonics in Fig. 11. An indicator W is used to quantify the energy level transferred from the fundamental waves to different higher-order harmonics. W is defined as the integral area between the higher-order harmonic amplitudes of the nonlinear system ($A_{\text{nonlinear}}{}^{n\text{th}}$) and its linear counterpart ($A_{\text{linear}}{}^{n\text{th}}$), written as $\int(A_{\text{nonlinear}}{}^{n\text{th}}$-

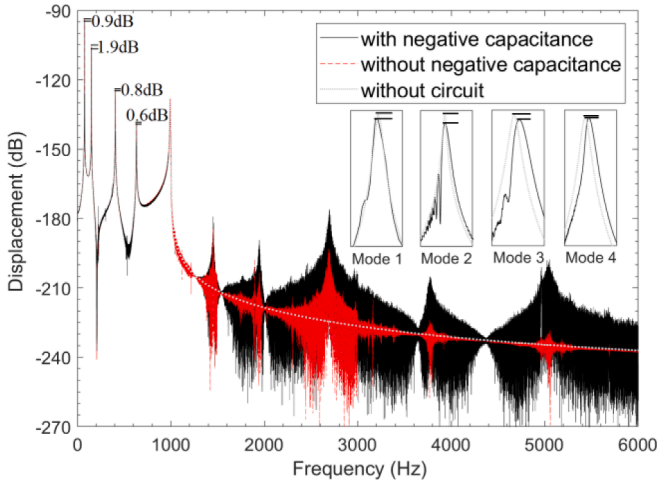

Fig. 12. Comparison of beam displacement spectrum envelopes under 0–1000 Hz sweep-frequency excitation force with different electrical circuits.

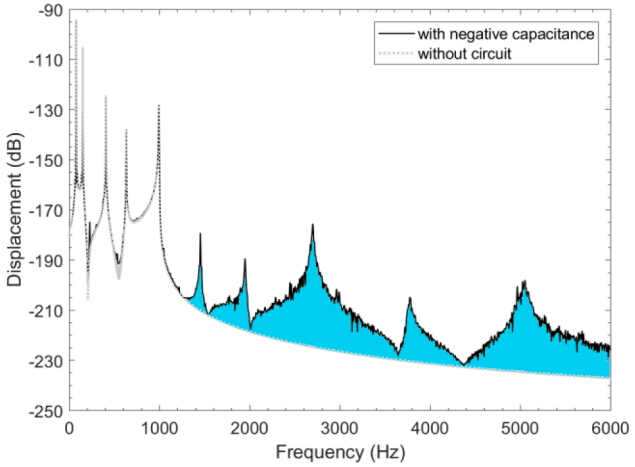

Fig. 13. Schematic diagram of increased energy at high frequencies, marked by blue shadow.

$A_{\text{linear}}{}^{n\text{th}})df$ [27]. We can see that enhancing the electromechanical coupling, the energy W contained in the 3rd to 7th harmonics also increase, which proves that enhanced electromechanical coupling effect can generate stronger higher-order harmonics, resulting in more significant energy increase at high frequencies. Since the energy level contained in the 7th harmonic is much lower than the first two lower-order harmonics, we will not consider it in the following discussion.

Next, the displacement spectrum of the ABH beam under different electrical conditions are considered to examine the outcome of the enhanced electromechanical coupling in term of ET effect. The beam is driven by the same excitation force used in the benchmark case. Fig. 12 shows that high-frequency resonance peaks emerge after 1000 Hz after the deployment of the electrical shunt, with or without the negative capacitance. Obviously, the high-frequency energy level of the system with the negative capacitance is further increased after 1000 Hz: an increase of the peak levels alongside a spreading out of the energy distribution. Note the absence of the damping in the damping layer explains the increase of the high frequency vibration level, which, as to be demonstrated later, is expected to be effectively absorbed when the damping of the layers is added. In addition to further confirming the expected ET enhancement due to the use of negative capacitance, Fig. 12 also shows a further reduction in the amplitudes of the first four resonance peaks before f_c, amounting to 2 dB reduction compared to the system without electrical shunt. This can also attribute to the fact that part of the low frequency energy is transferred to higher frequencies due to the enhanced nonlinear strength in the system. Despite the simplicity of the circuit design, the amplitude reduction for low-order modes is still a few decibels. The advantage of the proposed method based on ABH is its robustness for achieving broadband vibration reduction. The control effect is expected to be enhanced through more sophisticated circuit design or other means like nonlinear mechanical coupling.

For a quantitative assessment of the above effects, two indicators are respectively defined to measure the decreased energy at low frequencies and the transferred energy to high frequencies. For the former, the resonant peak level difference in the beam displacement spectra, ΔA, is used. For the latter, the increased energy at high frequencies is quantified by the integrated area, W_{ET}, between the beam

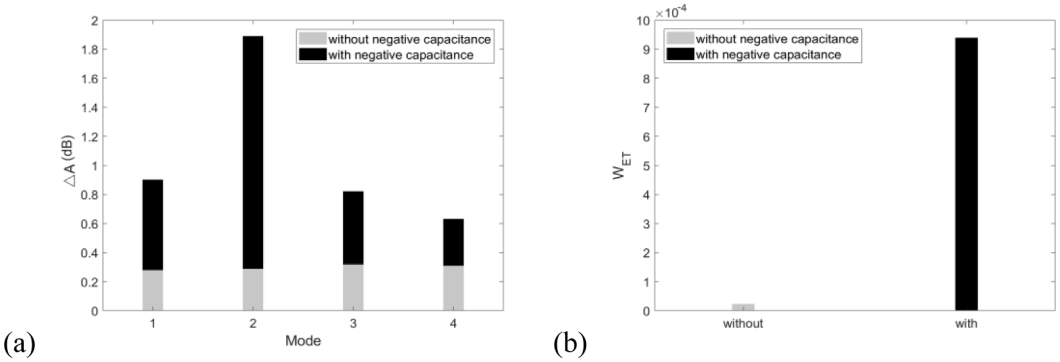

Fig. 14. Comparison of (a) reduced amplitudes ΔA of the low-frequency resonance peaks; and (b) increased energy W_{ET} in the high frequencies with and without negative capacitance.

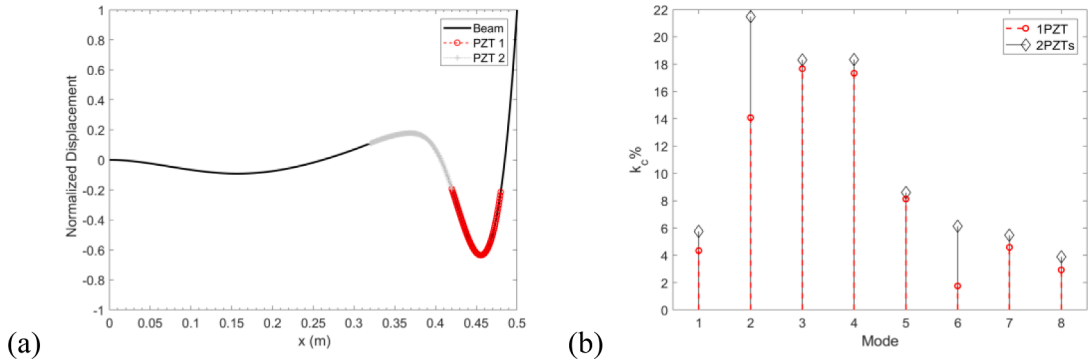

Fig. 15. (a) Mode shape of the fourth mode with two sets of PZTs covering the red part and the gray part, respectively; (b) electromechanical coupling factors with one and two sets of PZTs connected to the nonlinear shunt with negative capacitance.

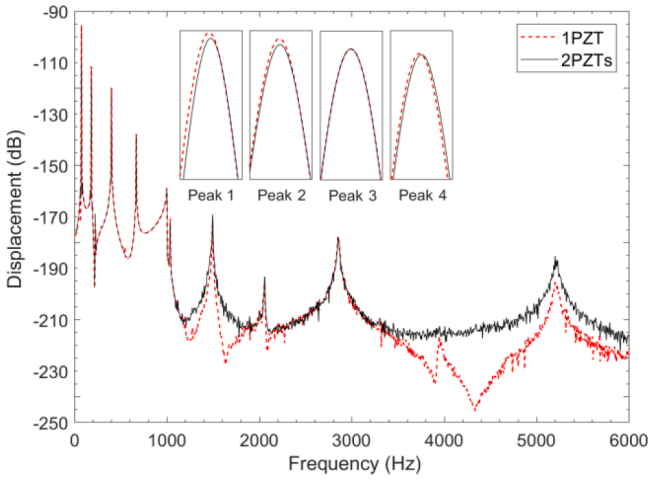

Fig. 16. Comparison of beam displacement spectrum envelopes under 0–1000 Hz sweep-frequency excitation force with one and two sets of PZTs connected to the nonlinear shunt with negative capacitance.

displacement response envelopes of the linear and nonlinear system, which emerges after the use of nonlinear shunt (the blue shadow part shown in Fig. 13). Obviously, since the energy contained in the excitation stops at 1000 Hz, W_{ET} can only be caused by the transferred energy.

Figs. 14(a) and 14(b) respectively show the variation of ΔA and W_{ET} with and without negative capacitance. Both parameters follow the same increasing trend, when adding the negative capacitance as a result of the enhanced electromechanical coupling.

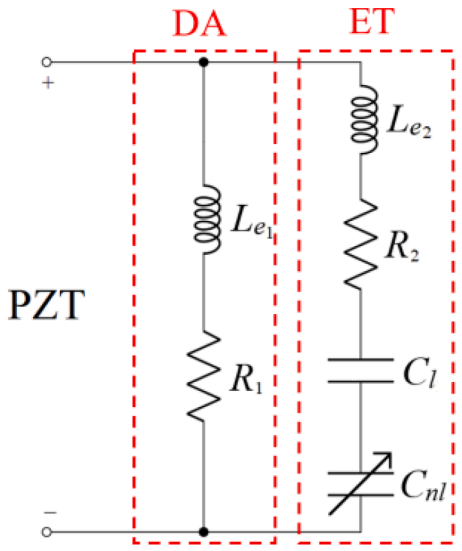

Fig. 17. Schematic diagram of nonlinear shunt with two electrical branches containing different functions.

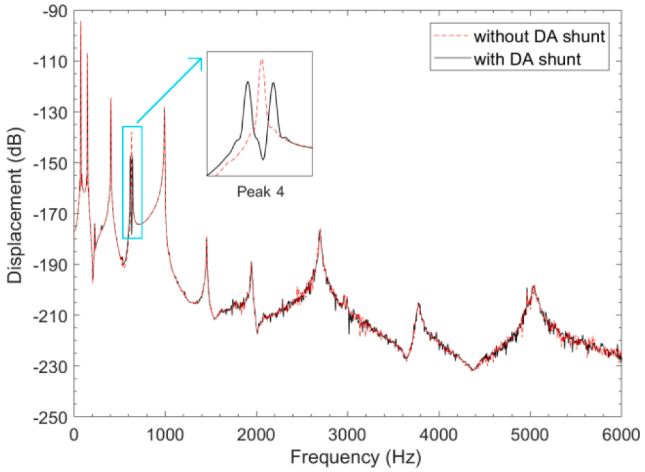

Fig. 18. Comparison of beam displacement spectrum envelopes under 0–1000 Hz sweep-frequency excitation force with and without DA shunt.

Typically, ΔA further increases by roughly 0.4 dB to 1.5 dB, and W_{ET} by a factor of 40 when a negative capacitance is introduced.

3.2.2. Multiple PZT pairs with negative capacitance in the shunt

Using multiple sets of PZTs can also help achieve the same objective for the ultimate purpose of achieving enhanced ET. As an example, an additional set of PZT patches is added to the beam discussed above containing already the first set of PZT. This second set of PZT is installed at the position where the fourth modal deformation is also large, $x_p = 0.32$m-0.42 m, as shown in Fig. 15(a). Using the same external shunt connected to each set of PZTs, the resultant k_c for the first eight structural modes is shown in Fig. 15(b), which also shows a slight increase in the coupling strength.

Fig. 16 compares the displacement spectrum envelopes of the beam with one and two sets of PZTs connected to the nonlinear shunt with negative capacitance. Again, in the targeted ET region beyond 1000 Hz, the one with two sets of PZTs obviously outperforms the one with only one PZT set, especially in the high frequency region above 3500 Hz. Meanwhile, the close-up insets of the first four resonance peaks also show a slightly decrease of the low-frequency vibration at structural resonances owing to the increasing PZT numbers. Therefore, as long as the electromechanical coupling is increased, either by introducing negative capacitance in the shunt (discussed in Section 3.2.1) or increasing PZT patches, enhanced low-to-high frequency ET can be materialized inside the ABH beam.

3.3. Dynamic absorber effects for lower-order resonances

The numerical examples in the previous section demonstrate that, although nonlinear shunts, especially with the negative

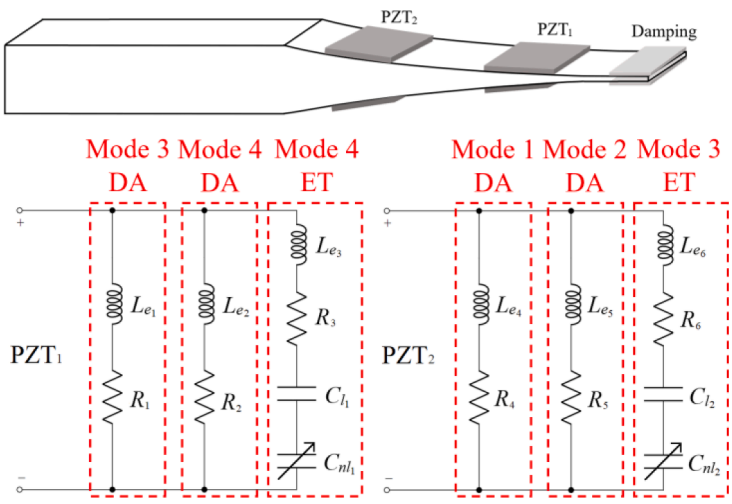

Fig. 19. Schematic diagram of designed electromechanical ABH beam with one set of damping layers and two sets of PZTs connected designed nonlinear shunt.

Table 2
Electrical parameters of designed circuit.

Electrical parameters
Inductance
$L_{e1} = 4.728$ H $L_{e2} = 1.688$ H $L_{e3} = 0.02$ H $L_{e4} = 81.4$ H $L_{e5} = 13.65$ H $L_{e6} = 0.02$ H
Resistance
$R_1 = 150\ \Omega$ $R_2 = 20\ \Omega$ $R_3 = 10\ \Omega$ $R_4 = 400\ \Omega$ $R_5 = 100\ \Omega$ $R_6 = 10\ \Omega$
Capacitance
$C_{l1} = -3.4005 \times 10^{-8}$ F $C_{l2} = -5.6399 \times 10^{-8}$ F $C_{nl1} = 1 \times 10^{-22}$ C^3V^{-1} $C_{nl2} = 1 \times 10^{-22}$ C^3V^{-1}

capacitance in multiple PZT patch settings, entail effective and beneficial ET to higher frequencies, the direct effects of the shunting on low frequency resonant vibration reductions are rather marginal. Therefore, in this section, we will explore ways to enhance the ET while maintaining the dynamic absorber (DA) effect to cope with the vibration mitigation at low-frequencies. Here, we still take a single set of piezoelectric shunts as an example to illustrate the idea by knowing that increasing PZT patches can naturally lead to better control performance. To tackle the problem, a linear electrical resonant branch is added to the previous nonlinear shunt, as shown in Fig. 17. The linear branch is designed to target one structural resonance through creating classical DA effects, while the remaining nonlinear branch is used for ET.

Fig. 18 shows the displacement spectrum envelopes of the beam used above with and without the additional DA branch in the electrical shunt. The linear DA branch is designed to target the fourth mode of the beam. It can be seen that the addition of the linear DA branch exerts nearly no effect on the high-frequency vibration caused by the previously observed ET. However, typical DA effects are apparent, which leads to a split of the resonance peak and a significant reduction (close to 10 dB) of the vibration level, as shown by the enlarged view of the fourth peak. This way, even in the presence of a strong electrical nonlinearity, dynamic absorber effect can still be maintained in the system owing to the linear DA branch of the shunt. Interesting enough, the two branches, linear and nonlinear, do not seem to interfere much with each other, reflecting a weak coupling between them. The benefit of this observation is that each branch can be designed separately and tactically to achieve their respective functions: linear part for low-frequency DA effect and the nonlinear part for cross-frequency ET effect. This solution allows for alleviating the detuning problem of the nonlinear shunts for low-frequency vibration mitigation, and the avoidance of linear DA failure in the presence of strong nonlinearity in the electrical shunts.

4. Comprehensive design

The above analyses demonstrate the possibility of enhancing the cross-frequency energy transfer by increasing the electromechanical coupling strength through different methods while maintaining the dynamic absorber effect to cope with low-frequency vibrations through adding the additional electrical branch. In this section, we will deploy this combined ET and DA design methodology and apply different strategies to different frequency bands to finally achieve broadband multimodal vibration mitigation. As an example, we use the same mechanical configuration of the electromechanical ABH beam used in Section 3.2.2, excited by the same external force (capped at 1000 Hz).

Though always present, the damping of the damping layers placed at the tip area of the beam, will be turned off and on purposely to facilitate analyses. Since systematic ABH effect is expected to appear starting from the fifth mode. Therefore, the high-frequency

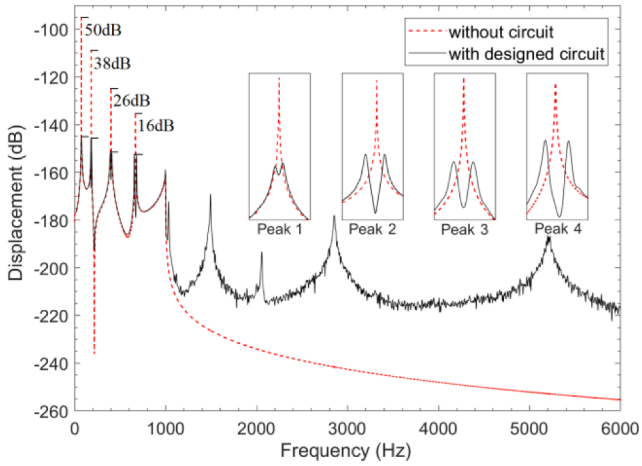

Fig. 20. Comparison of beam displacement spectrum envelopes under 0–1000 Hz sweep-frequency excitation force without circuit and with designed circuit.

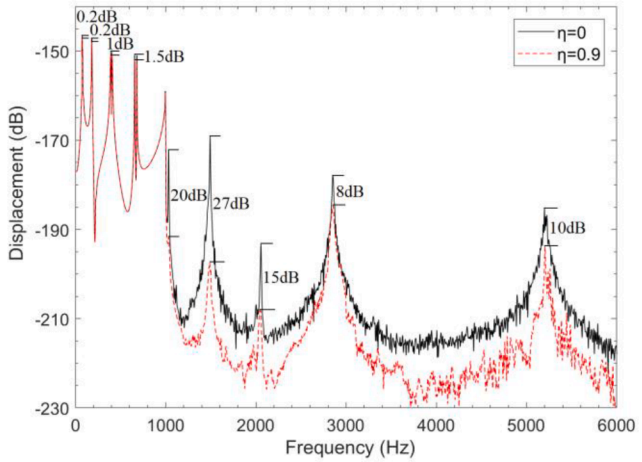

Fig. 21. Comparison of beam displacement spectrum envelopes under 0–1000 Hz sweep-frequency excitation force with different damping ratio η.

energy is expected to be dissipated by the ABH-enhanced damping effects. Therefore, we only need to design proper external circuit to cope with the first four structural modes before f_c. The electrical shunts are designed according to the following principles. For the 3rd and 4th modes in the frequency range from $1/3\,f_c$ to f_c, since the dominant harmonics of these modes (starting from the third harmonic onwards) would exceed the frequency barrier imposed by f_c, electrical branches will be designed to generate ET in the surrounding frequencies to a higher frequency region (above f_c) to facilitate the ABH-enhanced damping dissipation. To simultaneously reduced their own resonant responses, DA effects can also be embedded for these two modes although ET is the first concern. As to the first two modes, however, since their natural frequencies $f_n < 1/3\,f_c$, their third harmonics would still be lower than f_c, so that vibration mitigation of these modes have to totally rely on the DA effects. Following this design philosophy, corresponding circuit diagrams in the piezoelectric shunts are shown in Fig. 19. In the present case, two sets of PZTs are used, with the electrical parameters of the designed multi-branched shunts listed in Table 2. PZT-1 target the ET for the third mode through the nonlinear branch with negative capacitance while ensuring DA effects for modes 1 and 2 through its linear resonant brunches. PZT-2 ensures ET for mode 4 while exerting DA effects on both modes 3 and 4. The expected outcome is an effective ET from modes 3 and 4 and a systematic DA effect for all four structural modes.

Analyses on the achieved results are conducted in two stages. Firstly, in order to better show the ET process, the damping of the damping layers is deactivated ($\eta = 0.9$). Displacement spectra of the beam with and without the circuit are shown and compared in Fig. 20, which displays the expected ET effect to high frequencies and the DA effect for low-frequency modes. More specifically, compared with the system without shunts, vibration increases significantly in the targeted ET region beyond 1000 Hz, as evidenced by the significant increase in the energy level (due to the absence of the damping in the damping layers). Meanwhile, significant DA effects take place and split the first four resonant peaks apart, typical of DA effects, to yield a significant vibration reduction, ranging roughly from 16 dB to 50 dB.

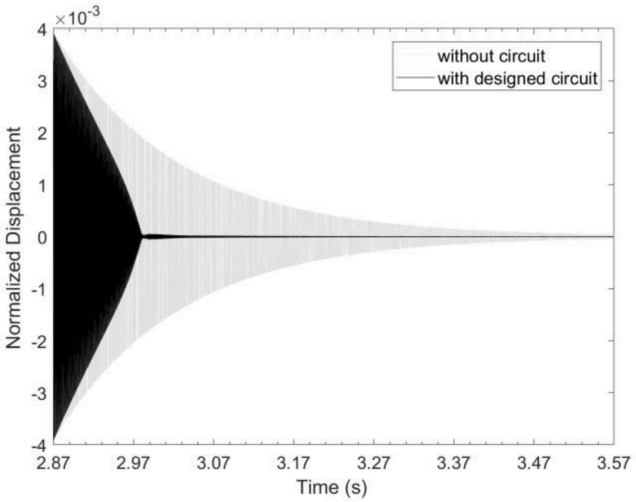

Fig. 22. Comparison of normalized beam displacement under 993.8 Hz single-frequency excitation force without and with designed circuit.

The damping of the damping layers is then activated through setting $\eta = 0.9$. This helps better apprehend the complete ABH process. Comparisons between the two cases ($\eta = 0$, 0.9) are made in Fig. 21. It can be seen that the activated damping effectively absorbs the transferred energy in the high frequency region above *fc*, leading to a significant vibration reduction there. The reduction is particularly impressive in the range of 1000–2000 Hz amounting to 27 dB, where locate the third harmonics of the 3rd and the 4th modes. Note the addition of the damping does not obviously jeopardize the vibration reduction of the lower-order resonances, although a slight reduction up to 1.5 dB is noticed. It is relevant to note that ABH-enhanced damping effect in different frequency bands also depends on the layout and the installation position of the damping layers, which is analogous to PZT (detailed discussion can be found in our previous paper [25]). The observed vibration reduction due to the addition of the damping layer reflects the entire ABH process, which is enhanced by the electrical nonlinearity through effective ET. The outcome of the overall electromechanical ABH process, owing to the combined DA and ET effects lower the effective frequency range of the ABH, allowing for broadband vibration mitigation.

To better show the energy evolution process, we excite the beam by a single-frequency force at the fifth resonance frequency, stop it after the beam reaches a steady state (here, the excitation stops at $t = 2$ s). This is to examine the free vibration response to better appreciate the advantages of the energy transfer more clearly using time-domain response. The time-domain signals of the beam displacement are normalized to their respective maximum values, as shown in Fig. 22. We note that at $t = 2.87$ s, the amplitudes of both cases are almost same, but after it, the vibration of the system with the designed circuit decays rapidly, evidencing a rapid energy flow from the beam to the electrical shunt. As a result, vibration attenuation of the beam is accelerated due to the increasing damping.

Finally, we conduct a wavelet transform (WT) near each of the first four resonance peaks. The wavelet transform is conducted in MATLAB by using the CWT function (as shown in Fig. 23), which is dedicated to analyze time-dependent frequency signals. Such analysis allows for a clear visualization of energy transfer inside a dynamic system with respect to time. In the present case in Fig. 23, the horizontal axis stands for the frequency of the sweeping excitation. The vertical axis is the frequency content of the system response.

More specifically, with the sweeping frequency around the first mode, Figures 23(a) and (e), show the WT spectra for linear and nonlinear cases, respectively. In both cases, high energy concentration is obviously around this mode, whereas higher-frequency components are rather small. More or less the same applies to the second mode. When the third and fourth modes are directly excited, the energy level at higher frequencies obviously increases in the nonlinear system (Figures 23(g) and (h)), but not in its linear counterpart (shown in the left column). These observations evidence clear energy transfer taking place inside the nonlinear system, suggesting that most high-frequency energy is indeed transferred from the third and fourth modes (the targeted modes) for which the electrical shunts are designed to produce the ET branches shown in Fig. 9. The process effectively enables controllable and targeted energy transfer.

The above numerical analyses show that not only the dynamic absorber effects can be flexibly tuned to achieve multi-modal vibration mitigation, but also the cross-frequency energy transfer be manipulated.

5. Conclusion

The content of this paper falls into our general efforts in imposing intentional electrical nonlinearities via PZT patches over an ABH beam to tactically influence its dynamics through electromechanical coupling for achieving broadband vibration mitigation. To overcome the existing limitations revealed by our experimental results, we firstly propose to enhance the cross-frequency energy transfer (ET) in the ABH beam through increasing the electromechanical coupling strength by using either multiple sets of PZTs or

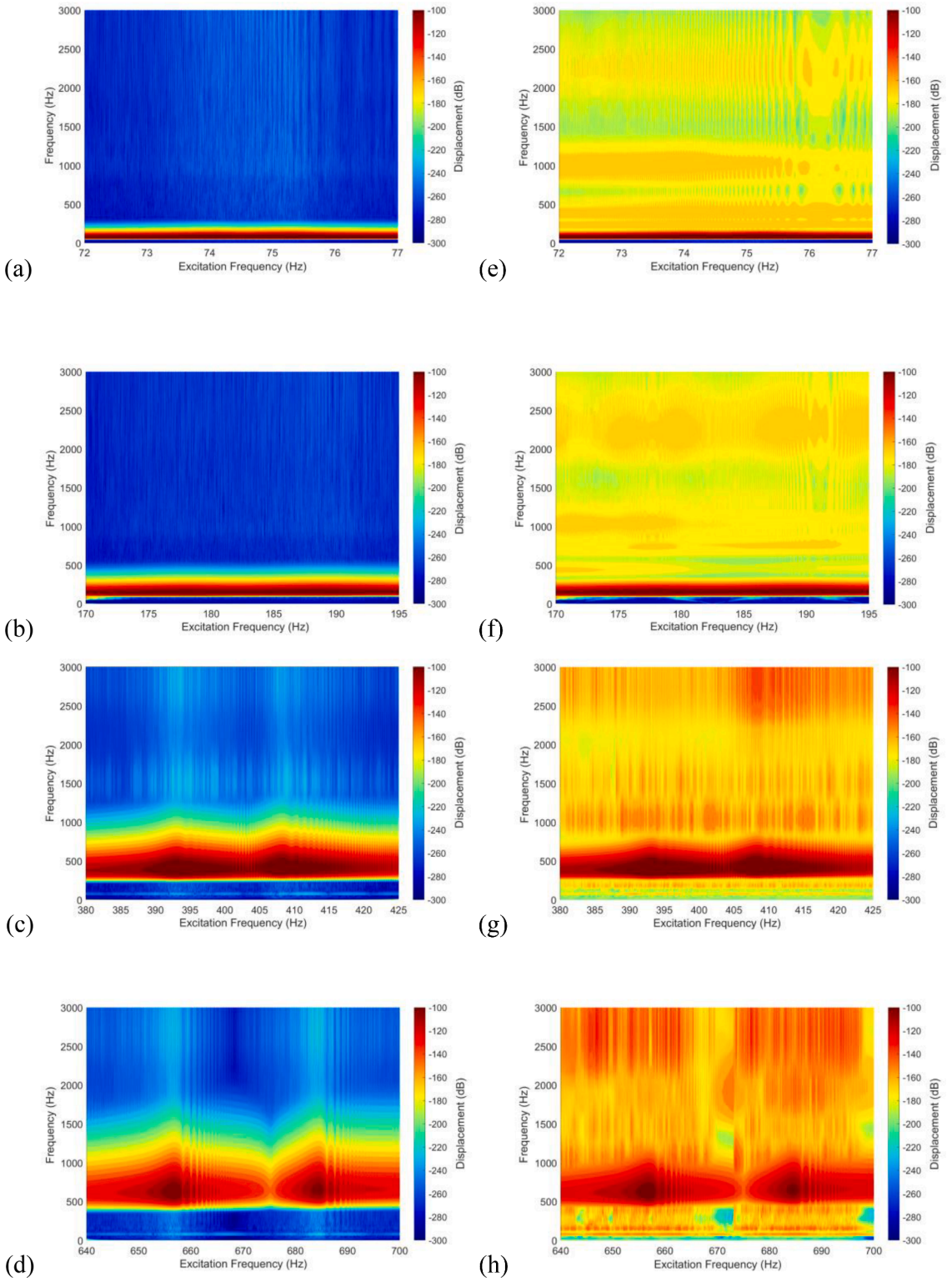

Fig. 23. Wavelet transformed 2D plot of the first four peaks with linear (left column) and nonlinear shunts (right column).

introducing a negative capacitance in the nonlinear shunt. Numerical examples show enhanced ET, despite rather marginal reduction of low frequency resonant vibration. To tackle the problem, linear electrical resonant branches are added to the nonlinear shunt to generate dynamic absorber (DA) effects without compromising the nonlinearity-dominated ET. It is demonstrated that the two

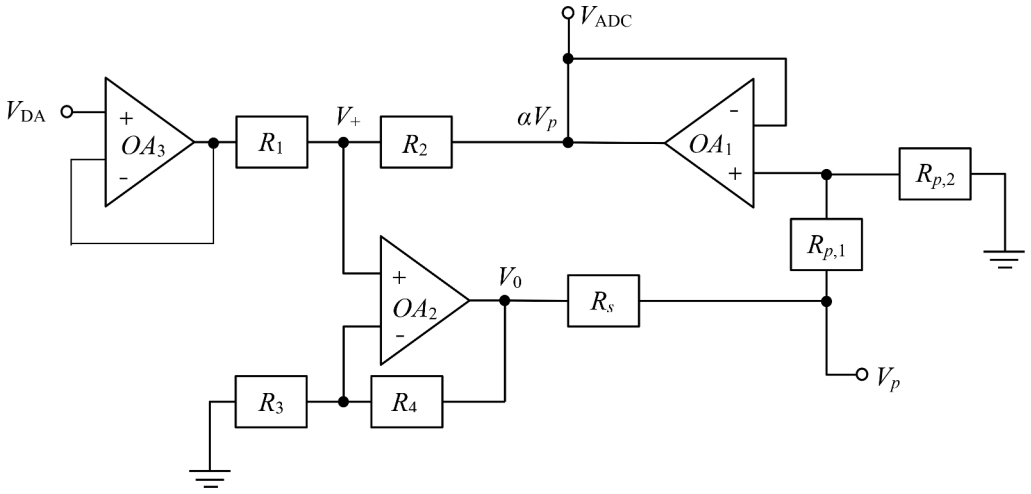

Fig. A.1. Circuit diagram of the digital vibration absorber [33].

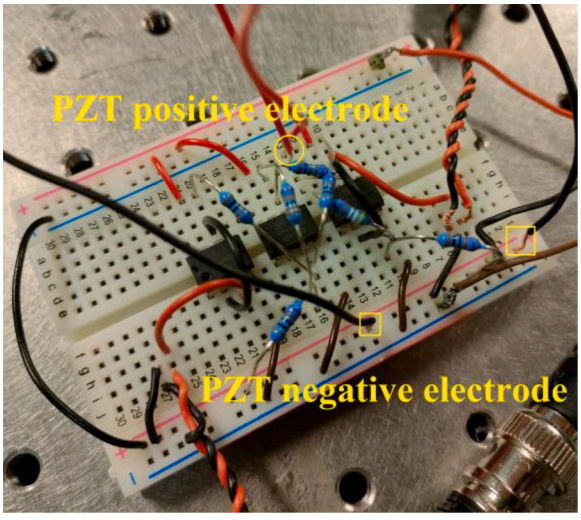

Fig. A.2. Prototype of the digital vibration absorber that is used in the experimental test.

parallelly arranged branches in a shunt, linear and nonlinear, are weakly coupled and can be separately designed to target particular modes to achieve pre-set functionalities. More specifically, we provide a comprehensive design example, which embraces the principle of ET and DA, deployed to cope with different frequency bands.

More specifically, the proposed vibration mitigation method roots in the following rationale. 1). High-frequency vibration energy, typically above f_c, can be naturally dissipated by the ABH-enhanced damping in the system, exemplified by a small amount of damping materials placed at the ABH tip region. 2). For the frequency range below but relatively close to f_c, typically from $1/3\,f_c$ to f_c, nonlinear electrical shunts can be deployed to achieve ET to a higher frequency region (above f_c) so that the same energy dissipation process (summarized in 1) above) can be subsequently triggered. 3). For the lower-order resonant modes, vibration mitigation would mainly rely on the DA effects achieved through the linear resonant branches in the shunt. Note DA effects can also be imposed to these modes belonging to the category 2) above without sensibly affecting the expected ET. The outcome of this comprehensive design is the breaking down of the frequency barrier existing in conventional linear ABH structures, and appreciable broadband multi-modal vibration mitigation at low frequencies.

Declaration of Competing Interest

The authors declare that they have no known competing financial interests or personal relationships that could have appeared to influence the work reported in this paper.

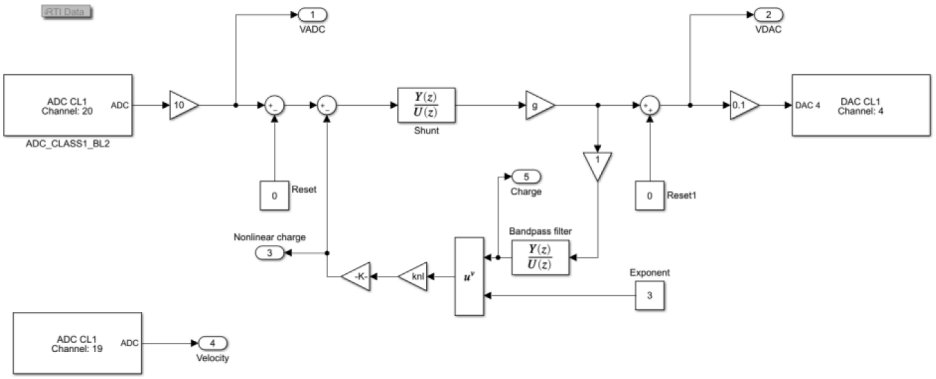

Fig. A.3. Block diagram representation of the input/output relation in the digital system.

Data availability

No data was used for the research described in the article.

Acknowledgements

Authors thank the Research Grant Council of the Hong Kong SAR (PolyU 152023/20E) for financial support.

Appendix A. Diagrams of Digital Vibration Absorber in Experimental Tests

References

[1] A. Pelat, F. Gautier, S.C. Conlon, F. Semperlotti, The acoustic black hole: A review of theory and applications, J. Sound Vib. 476 (2020), 115316.
[2] H. Ji, W. Huang, J. Qiu, L. Cheng, Mechanics problems in application of acoustic black hole structures, Adv. Mech. 47 (2017) 333.
[3] M. Mironov, Propagation of a flexural wave in a plate whose thickness decreases smoothly to zero in a finite interval, Sov. Phys. Acoust. 34 (1988) 318–319.
[4] V.V. Krylov, On the velocities of localized vibration modes in immersed solid wedges, J. Acoust. Soc. Am. 103 (1998) 767–770.
[5] V.V. Krylov, New type of vibration dampers utilising the effect of acoustic 'black holes, Acta Acust. United Ac. 90 (2004) 830–837.
[6] D. O'Boy, V.V. Krylov, Damping of flexural vibrations in circular plates with tapered central holes, J. Sound Vib. 330 (2011) 2220–2236.
[7] S.C. Conlon, J.B. Fahnline, F. Semperlotti, Numerical analysis of the vibroacoustic properties of plates with embedded grids of acoustic black holes, J. Acoust. Soc. Am., 137 (1), 447-457.
[8] L. Tang, L. Cheng, Ultrawide band gaps in beams with double-leaf acoustic black hole indentations, J. Acoust. Soc. Am. 142 (2017) 2802–2807.
[9] L. Tang, L. Cheng, Enhanced acoustic black hole effect in beams with a modified thickness profile and extended platform, J. Sound Vib. 391 (2017) 116–126.
[10] T. Zhou, L. Cheng, A resonant beam damper tailored with acoustic black hole features for broadband vibration reduction, J. Sound Vib. 430 (2018) 174–184.
[11] P.A. Feurtado, S.C. Conlon, Transmission loss of plates with embedded acoustic black holes, J. Acoust. Soc. Am. 142 (2017) 1390–1398.
[12] L. Ma, L. Cheng, Sound radiation and transonic boundaries of a plate with an acoustic black hole, J. Acoust. Soc. Am. 145 (2019) 164–172.
[13] L. Zhao, S.C. Conlon, F. Semperlotti, Broadband energy harvesting using acoustic black hole structural tailoring, Smart Mater. Struct. 23 (2014), 065021.
[14] H. Ji, Y. Liang, J. Qiu, L. Cheng, Y. Wu, Enhancement of vibration based energy harvesting using compound acoustic black holes, Mech. Syst. Sig. Process. 132 (2019) 441–456.
[15] V.V. Krylov, Acoustic black holes: recent developments in the theory and applications, IEEE Trans. Ultrason. Ferroelectr. Freq. Control 61 (2014) 1296–1306.
[16] B.M.P. Chong, L.B. Tan, K.M. Lim, H.P. Lee, A review on acoustic black-holes (ABH) and the experimental and numerical study of ABH-featured 3D printed beams, Int. J. Appl. Mech. Eng. 9 (2017), 1750078.
[17] J.Y. Lee, W. Jeon, Vibration damping using a spiral acoustic black hole, J. Acoust. Soc. Am. 141 (2017) 1437–1445.
[18] X. Jia, Y. Du, K. Zhao, Vibration control of variable thickness plates with embedded acoustic black holes and dynamic vibration absorbers, in: ASME 2015 Noise Control and Acoustics Division Conf. at InterNoise, 2015.
[19] L. Zhao, Low-frequency vibration reduction using a sandwich plate with periodically embedded acoustic black holes, J. Sound Vib. 441 (2019) 165–171.
[20] Y. Zhang, K. Chen, S. Zhou, Z. Wei, An ultralight phononic beam with a broad low-frequency band gap using the complex lattice of acoustic black holes, Appl. Phys. Express 12 (2019), 077002.
[21] A.H. Nayfeh, D.T. Mook, P. Holmes, Nonlinear Oscillations, Wiley, New York, 1979.
[22] A. Nayfeh, R. Ibrahim, Nonlinear interactions: analytical, computational, and experimental methods, Appl. Mech. Rev. 54 (2001) B60–B61.
[23] F. Nucera, A.F. Vakakis, D. McFarland, L. Bergman, G. Kerschen, Targeted energy transfers in vibro-impact oscillators for seismic mitigation, Nonlin. Dyn. 50 (2007) 651–677.
[24] V. Denis, A. Pelat, C. Touzé, F. Gautier, Improvement of the acoustic black hole effect by using energy transfer due to geometric nonlinearity, Int. J. Non Linear Mech. 94 (2017) 134–145.
[25] V.E. Gusev, C. Ni, A. Lomonosov, Z. Shen, Propagation of flexural waves in inhomogeneous plates exhibiting hysteretic nonlinearity: Nonlinear acoustic black holes, Ultrasonics 61 (2015) 126–135.
[26] H. Li, C. Touzé, F. Gautier, A. Pelat, Linear and nonlinear dynamics of a plate with acoustic black hole, geometric and contact nonlinearity for vibration mitigation, J. Sound Vib. 508 (2021), 116206.

[27] L. Zhang, G. Kerschen, L. Cheng, Nonlinear Features and Energy Transfer in an Acoustic Black Hole Beam through Intentional Electromechanical Coupling, Mech. Syst. Sig. Process.
[28] L. Zhang, G. Kerschen, L. Cheng, Electromechanical Coupling and Energy Conversion in a PZT-Coated Acoustic Black Hole Beam, Int. J. Appl. Mech. Eng. 12 (2020), 2050095.
[29] Y. Wang, J. Du, L. Cheng, Power flow and structural intensity analyses of acoustic black hole beams, Mech. Syst. Sig. Process. 131 (2019) 538–553.
[30] T. Detroux, L. Renson, L. Masset, G. Kerschen, The harmonic balance method for bifurcation analysis of large-scale nonlinear mechanical systems, Comput. Meth. Appl. Mech. Eng. 296 (2015) 18–38.
[31] S.Y. Chang, Studies of Newmark method for solving nonlinear systems: (I) basic analysis, J. Chin. Inst. Eng. 27 (2004) 651–662.
[32] G. Raze, A. Jadoul, S. Guichaux, V. Broun, G. Kerschen, A digital nonlinear piezoelectric tuned vibration absorber, Smart Mater. Struct. 29 (2019), 015007.
[33] A.J. Fleming, S. Behrens, S.O.R. Moheimani, Synthetic impedance for implementation of piezoelectric shunt-damping circuits, Electron. Lett. 36 (18) (2000) 1525.